Electrocatalysis of the nitrite reduction : a mechanistic study

Duca, M.

7

Electrocatalytic reduction of nitrite on transition and coinage metals

Abstract

A systematic comparison of the electrochemical reduction of nitrite at polycrystalline metals has been carried out. In acidic media, solution-phase NO from HNO_2 decomposition is converted to N_2O by all noble metals in a common potential range for most metals (0.2 – 0.5 V vs. RHE). Transition metals can also convert HNO_2 directly to hydrogenated products (NH_3OH^+, NH_4^+) at lower potentials, while coinage metals (Ag, Au, Cu) feature a stepwise reduction to NO and N_2O, which can be both detected by on-line mass spectrometry. The reduction of nitrite ions in alkaline media never yields gaseous products; the first electron transfer to give adsorbed NO is the rate-determining step for all noble metals. Coinage metals are largely inactive, except for Cu. The selectivity and electrocatalytic trends have been interpreted based on DFT calculations of the metal-NO interaction available in the literature. In agreement with the Sabatier principle, metals with an intermediate affinity to NO are the most reactive and show the lowest tendency to poisoning. Coinage metals are a special case because of their weak NO adsorption and the formation of NO dimers.

This chapter has been accepted for publication in *Electrochimica Acta*.

7.1 Introduction

Overfertilization is the main cause of the current global imbalances in the nitrogen cycle[1,2], leading to the accumulation of potentially toxic nitrate and nitrite ions [3] in the groundwater. For this reason, the levels of these anions must be measured accurately with analytical techniques [4] and various wastewater remediation techniques have to be developed [5-9]. Electrochemical processes [10] cannot yet achieve sufficient selectivity for a large-scale commercial implementation, as byproducts such as N_2O or NH_3 [11] are often generated, which are more dangerous than the targeted pollutants. The desired electrochemical N_2 formation usually involves the stepwise reduction NO – N_2O – N_2, for metal and biological systems alike [11-13], but it may also be achieved by exploiting a shortcut of the nitrogen cycle involving the recombination of NH_x and NO (adsorbed) species (Chapter 3 and 4), which are generated from nitrite on Pt (100) in alkaline conditions.

Nitrite is an important species from the point of view of the electrochemical nitrogen cycle [11], as it is an intermediate in NO oxidation [14] and NO_3^- reduction [15]. In aqueous solutions, nitrite displays pH-dependent homogeneous-phase equilibria, such as the acid-base equilibrium HNO_2/NO_2^- (p*K*a = 3.16 [16], 3.37 [17]) .Therefore NO_2^- predominates in neutral/alkaline pH media, while HNO_2 is the dominant species at pH < 2; accordingly, the electrochemical response of an electrode material will be greatly affected by the shift from HNO_2 to NO_2^- (Chapters 2,6 and 8). Besides, HNO_2 decomposes to NO in acidic media [11,18], which is a reactive molecule on most metal and non-metal electrodes [11] (see also Chapters 2, 6 and 8).

Transition and coinage metal electrodes have been widely investigated in terms of their reactivity towards the reduction of nitrate. Dima et al. have formulated a general mechanism in which the first step (NO_3^- to NO_2^-) has been recognized as rate determining for all metals in acidic media[15]. On the other hand, the analysis of the selectivity has shown that a soluble product (NH_4^+) predominates for most electrodes, while gaseous products can be detected only at a Cu electrode [15]. Copper is indeed the most studied among the coinage metals for applications in neutral and alkaline media [12,19-25]. It is characterized by a stepwise reaction converting nitrate to nitrite (which may adsorb and poison the copper surface) and subsequently to ammonia [23]. Additionally, a Cu-Pd bimetallic electrocatalyst shows a high selectivity to N_2 [12]. Silver displays a much lower catalytic activity for the reduction of nitrate in alkaline media, requiring high overpotentials[20].

Fewer works have focused on the reduction of HNO_2/NO_2^-, which is unfortunate as it is the selectivity-determining step of overall nitrate reduction[11]. In addition, the presence of HNO_2/NO_2^- as bulk reactant, and not only as (surface) short-lived intermediate, often brings about a modification of the selectivity compared to nitrate reduction, as testified by the more intense N_2O evolution on Pt and Rh electrodes during nitrous acid reduction in acidic media (Chapters 2 and 6). A more general study of the mechanism of nitrite reduction, directly comparing metals such as Ir, Ru, Pd and the coinage metals, is therefore desirable, in particular with regard to an accurate determination of the factors that influence product selectivity, such as the pH. Spectroelectrochemical studies of Ir electrodes have shown that some basal planes tend to dissociate NO in acidic media[26,27], with O_{ads} being the actual poison at the surface[28]. Spectroelectrochemistry also plays a central role in the investigation of NO/NO_2^- reduction at Ru film electrodes: Yan et al. [29] have shown that Ru tends to be covered by an NO adlayer replenished by solution-phase HNO_2. NO_{ads} can also coexist with Ru oxides at higher potentials. Nakata et al. have screened various noble metal electrodes for nitrite reduction in the presence and in the absence of a promoter (Sn) [30] using off-line analytical techniques in order to determine the reaction products quantitatively. In the potential region close to hydrogen evolution, Ir, Pt, Ru and Rh all convert NO_2^- to both soluble (NH_4^+) and gaseous products, while Pd stands out as the only metal with 100% selectivity to volatile products, i.e. N_2O and N_2. Remarkably, N_2 was detected independently of the electrode material.

We report here a study focused on nitrite/nitrous acid reduction on various metals, both with respect to the reaction mechanism and the product distribution. Pt and Rh were studied in detail in Chapters 2 and 6. The use of on-line analytical techniques, such as On-Line Electrochemical Mass Spectroscopy (OLEMS), has allowed us to highlight the evolution of gaseous products, which is of great interest in acidic solutions. We show that the formation of N_2O in acidic nitrite-containing solutions is a common feature of all noble metals; on the other hand, coinage metals preferentially evolve NO. In alkaline media, noble metals reduce nitrite to hydrogenated products via multistep mechanisms in which for all metals the rate-determining step is the first electron transfer.

7.2 Experimental

All glassware was cleaned following a standard procedure[31]. Suprapur (Merck) or comparably pure (Sigma-Aldrich) electrolytes and Millipore MilliQ water (resistivity >18.2 MΩ cm) were employed to prepare electrolyte solutions; prior to the experiments oxygen was removed by bubbling argon (purity grade 6.0) through the solution for at least 15 minutes (acidic solution) or 30 minutes for alkaline solutions. Argon blanketing was maintained over the solution during the experiments. $NaNO_2$ (99.999%, Sigma-Aldrich) was used as received and stored in a desiccator under vacuum; contact with air was kept as short as possible. In the pH range where nitrous acid decomposition takes place, concentrations reported in this paper are meant as nominal (initial); no real-time monitoring of the concentration was carried out in the present study. We have elsewhere shown that nitrous acid decomposition is enhanced by stirring, gas blanketing over the solution and increased acidity. The decomposition follows a second-order kinetics (Chapter 2). To minimize the effect of the decomposition, all experiments at acidic pH were performed immediately after the addition of nitrite to the acidic electrolyte. Phosphate buffer solutions (ionic strength 0.1 M) were prepared for experiments at pH 3; the pH was checked before and after the experiments with a Radiometer Copenhagen pH meter. No noticeable change was observed during the experiments.

An Autolab PGSTAT20 (bi-)potentiostat was used throughout this work. Transfer and stationary experiments were carried out with electrodes of various shapes (flag or bead), all at least 99.9% purity (various suppliers). The Au, Pd and Ir flag electrodes were flame-annealed and quenched in water saturated with an Ar atmosphere[15] or in air (Au). Ag electrodes were pretreated following a different procedure. The Ag counter electrode (see below) was polished with coarse emery paper and sonicated. The Ag working electrode, on the other hand, was polished with alumina of decreasing particle size until a mirror finish was obtained. Lastly, the Ag electrode was electrochemically activated by means of repeated cycling in a 0.1 M $HClO_4$ solution between the foot of the Ag oxidation peak and the hydrogen evolution[15], with an Ag electrode as counter, until a stable voltammogram was obtained. Only the polished part was exposed to the solution in a hanging-meniscus configuration. Ru was deposited on a gold bead following the procedure suggested by Weaver et al.[32], although a much longer deposition time was used to ensure a fully pinhole-free deposition. Pd deposition on Au was based on the work of the

Kolb group[33]. The metal was deposited as thin layers by repeated cycling in a 0.1 M H_2SO_4 solution containing 10^{-4} M or 10^{-5} M Pd^{+2} ions (for a RDE Au disk or a smaller Au bead, respectively) in the potential range 0.7 - 0.09 V at 20 mV s^{-1}. The deposition was stopped before bulk deposition (signaled by a large feature of hydrogen absorption) was achieved; the thickness of the thin Pd layer was not exactly determined but it can be estimated to ca.3 monolayers (ML); two potentiodynamic cycles were performed to obtain such result. Palladium was added as $PdSO_4 \cdot 2H_2O$ (99.95 %, Alfa Aesar). For all electrochemical experiments involving bulk Ir or Pd electrodes, the counter electrode was a Pt flag. In other cases, an Au electrode was preferably used. A Reversible Hydrogen Electrode (RHE) was employed as reference electrode for all experiments, and all potentials reported in this paper are referred to RHE.

Rotating gold disk electrodes (diameter 5 mm) were used in a Pine Instrument Ring-Disk Teflon tip equipped with a Pt ring; rotating disk (RDE) and rotating ring-disk (RRDE) experiments were performed with a Pine Instrument motor generator (MSR rotator). The experimental collection efficiency was 0.26 ± 0.03 as obtained with the reversible $[Fe(CN)_6]^{-4}/[Fe(CN)_6]^{-3}$ couple. A different cleaning procedure was used for the RRDE tip, as described in Chapter 2.

Adsorbate studies were performed using the following transfer procedure[34]: the flag electrode was immersed in a nitrite-containing solution (0.8 mM) of a chosen electrolyte under potential control for 120 seconds, rinsed and then protected with a droplet of water during the transfer to another cell containing clean electrolyte. Nitric oxide ad-layers thus formed are known to undergo the transfer unscathed [35]. The nitrite concentration chosen for the adsorption step equals the one used in stationary continuous reduction experiments (0.8mM).

On-Line Electrochemical Mass Spectrometry (OLEMS) [36] measurements were performed on an EvoLution mass spectrometer system (European Spectrometry Systems Ltd). The system consists of a Prisma QMS200 (Pfeiffer), brought to vacuum with a TMH-071P turbo molecular pump (60 l s^{-1}, Pfeiffer) and a Duo 2.5 rotary vane pump (2.5 m^3 h^{-1}, Pfeiffer). During measurements, the pressure inside the MS was 1 - 5 · 10^{-6} mbar. Pretreatment procedures and details can be found in Chapter 2. For OLEMS, bead type electrodes were used whenever available. OLEMS data in the paper are plotted as recorded or after noise filtering with commercial scientific data analysis software. It must be borne in mind that, due to

varying collection performances of every single OLEMS Teflon tip, a quantitative comparison of the various graphs is not directly possible.

7.3. Results

7.3.1 Acidic media

In the (mildly) acidic pH range it is more appropriate to refer to nitrous acid, as this is the predominant species[11]. The following subsections are ordered according to the different experimental techniques used.

7.3.1.1 Electrochemical measurements

Nitrite reduction was investigated at stationary electrodes in (mildly) acidic media (0.1 M or 0.5 M H_2SO_4, 0.1 M $HClO_4$ or 0.1 M phosphate buffer, pH 3). $HClO_4$ should preferentially be used to avoid anion interference. However, H_2SO_4 must be used as supporting electrolyte for Ir, as this metal catalyzes the decomposition of ClO_4^- anions to Cl^- [37], and it was also chosen for Ru, because adsorbed bisulfate exerts a protective action versus Ru oxidation[38] and for Pd, because Pd deposition on Au from sulphate-containing solution yields a better deposit than in the presence of chloride ions [33]. Fortunately, nitrite reduction in acidic media is not as sensitive to the nature of the anion of the supporting electrolyte as nitrate reduction [15] (Chapter 2).

7.3.1.1.1 Iridium

The voltammetric profile of an iridium electrode in 0.5 M H_2SO_4 is shown in Figure 1. The choice of 0.4 V as upper potential limit is dictated by the need to avoid the formation of Ir oxides: the onset of this process has been reported at 0.4 V [39]. The blank voltammogram is characterized by a main signal at 0.12 V which can be assigned to (110) sites [40], and a background contribution of other single-crystal orientations, with (100) domains giving rise to the minor feature observed at 0.29 V [26,40]. This blank voltammogram was obtained reproducibly with the flame-annealing procedure.

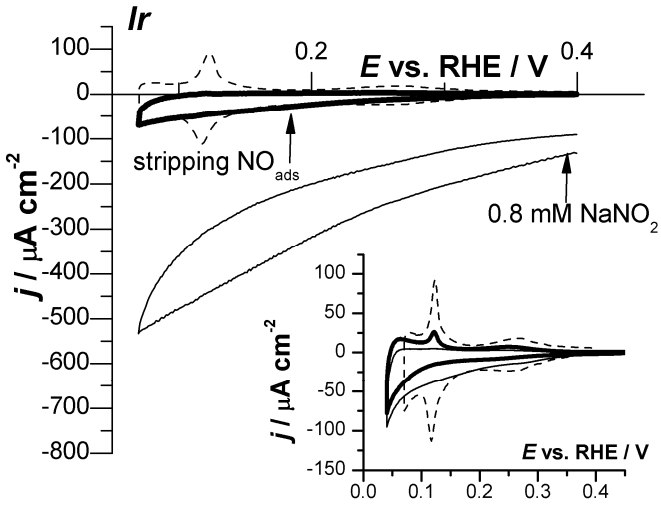

Figure 1 Voltammetric profiles for the reduction of 0.8 mM $NaNO_2$ in 0.5 M H_2SO_4 at a polycrystalline Ir electrode (continuous line) compared to the blank voltammogram (dashed line) and the first cycle of NO_{ads} stripping (bold line) in the same electrolyte, $v = 20$ mV s^{-1}. Inset: two cycles of NO_{ads} stripping (thin and bold lines, first and second respectively) when a different lower potential limit is used with respect to the main figure, compared to the blank (dashed line) in 0.5 M H_2SO_4, $v = 20$ mV s^{-1}.

Reduction currents were measured after the addition of $NaNO_2$: when the nitrite concentration is increased, the voltammetric profile becomes progressively dominated by a featureless reduction signal (see Figure 1). The nonzero current at the starting potential (0.4 V) indicates that reduction processes are already operative. Additional insight can be obtained by comparing the profile of the continuous reduction to the reductive stripping of NO_{ads}, which can be performed in a so-called transfer experiment (see experimental part). The first scan of the stripping experiment is also shown in Figure 1: it can be clearly seen that the typical features of the blank voltammogram have disappeared for the NO-covered electrode. Different to Pt or Rh, there is no real reduction peak, and the shape of the stripping scan closely resembles the featureless continuous nitrite reduction, albeit with lower currents. The blank voltammogram is not recovered within 5 scans when the potential limits used are 0.07 – 0.4 V, as for Figure 1. If the lower potential limit is extended 50 mV in the negative direction, as shown in the inset to Figure 1, the hydrogen adsorption signals of (110) sites voltammogram can partially be recovered after two consecutive cycles, whereas the small features

corresponding to (100) sites do not reappear. Even repeated cycling did not enable us to recover the blank voltammogram fully, thus testifying to the presence of a rather resilient adsorbed species.

7.3.1.1.2 Ruthenium

When studying the electrochemistry of a ruthenium electrode, one must always bear in mind that this metal shows an extremely high tendency to form an oxide layer, even at potentials neighboring the hydrogen adsorption region[29,38,41-44]. For this reason, we limited our investigation to a potential window where the presence of surface oxides is expected to be minimal, that is for $E < 0.20$ V in the absence of nitrite and $E < 0.35$ V in the presence of nitrite. Cai et al.[29] did not obtain spectroscopic evidence for oxide formation for $E < 0.3$ V in a 0.1 M $HClO_4$ solution containing 20 mM $NaNO_2$. Figure 2 shows the electrochemical response of a deposited Ru electrode in contact with a 0.5 M H_2SO_4 + 0.8 mM $NaNO_2$ solution. The featureless shape of the voltammetric profile in this acidic nitrite-containing solution is consistent with previous reports by Colucci et al. [42] concerning Ru electrochemistry in a NO-saturated solution and Ru nanofilm electrodes[29]. A stripping experiment was also carried out: the results are shown in the inset to Figure 2. The NO adlayer was completely removed after the first sweep and the profile of a clean Ru electrode was recovered, although with a decreased current density with respect to the first blank recorded after ruthenium deposition. This discrepancy may be ascribed to the fact that, when the electrode history is taken into account, the electrochemistry of ruthenium is fraught with irreproducibility, due to the facile formation of surface oxides [29]. A rotating ring-disk experiment was also carried out with a rotating ring-disk (RRDE) setup featuring an Ru-coated Au disk and a Pt ring in 0.5 M H_2SO_4 containing 50 μM $NaNO_2$. The ring electrode is extremely useful for the detection of a possible product (or intermediate), NH_3OH^+[45] (Chapter 2). The disk current was found to be only dependent on the rotation rate up to ω = 1400 rpm, reaching a constant value for higher rates, in contrast to the multi-electron diffusion-controlled conversion of HNO_2 typical of Pt and Rh (Chapters 2 and 6). Therefore, the data did not fit to the Levich and the Koutecky-Levich equations[46]. Shielding experiments with constant disk potentials in the range 0.07 – 0.01 V did not evidence the loop in the ring current signal typical of hydroxylamine production at the disk[45] (Chapters 2 and 8). Therefore, we exclude that HNO_2 can be converted to NH_3OH^+ at a Ru electrode.

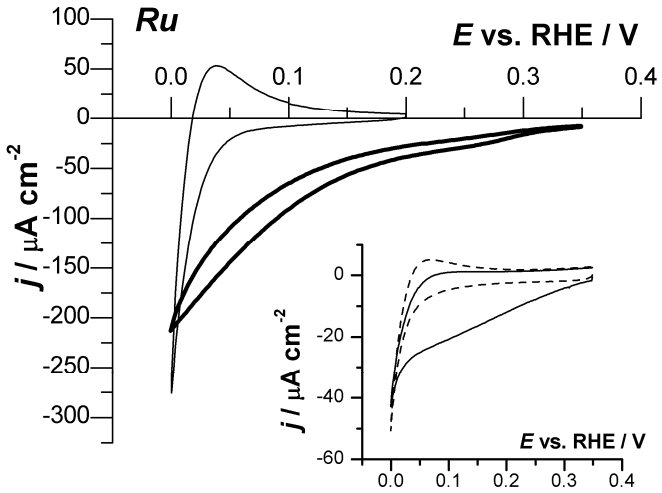

Figure 2 Voltammetric profiles for the reduction of 0.8 mM $NaNO_2$ in 0.5 M H_2SO_4 at a Ru film deposited on Au (bold line) compared to the blank voltammogram (thin line), v = 20 mV s^{-1}. Inset: first and second cycle of NO_{ads} stripping (thin and dashed lines, respectively) in 0.5 M H_2SO_4, v = 20 mV s^{-1}.

7.3.1.1.3 Thin-layer palladium on gold

Thin-layer palladium electrodes were first tested as stationary electrodes. The recorded voltammogram is very similar to the two-wave signal reported for the reduction of nitrite in acidic media on Pt (Chapter 2) (a voltammogram of a stationary Pd electrode can be found below in Figure 7A) and the onset of NO stripping is located at 0.175 V, a much lower potential than Pt (E_{onset} = 0.35 V for Pt – see Chapter 2). Further experiments were carried out with a rotating ring-disk electrode. Figure 3A displays the response of a thin-layer Pd rotating disk electrode to the reduction of 50 μM $NaNO_2$ in 0.1 M H_2SO_4 compared to Pt (in 0.5 M H_2SO_4 – see Chapter 2).

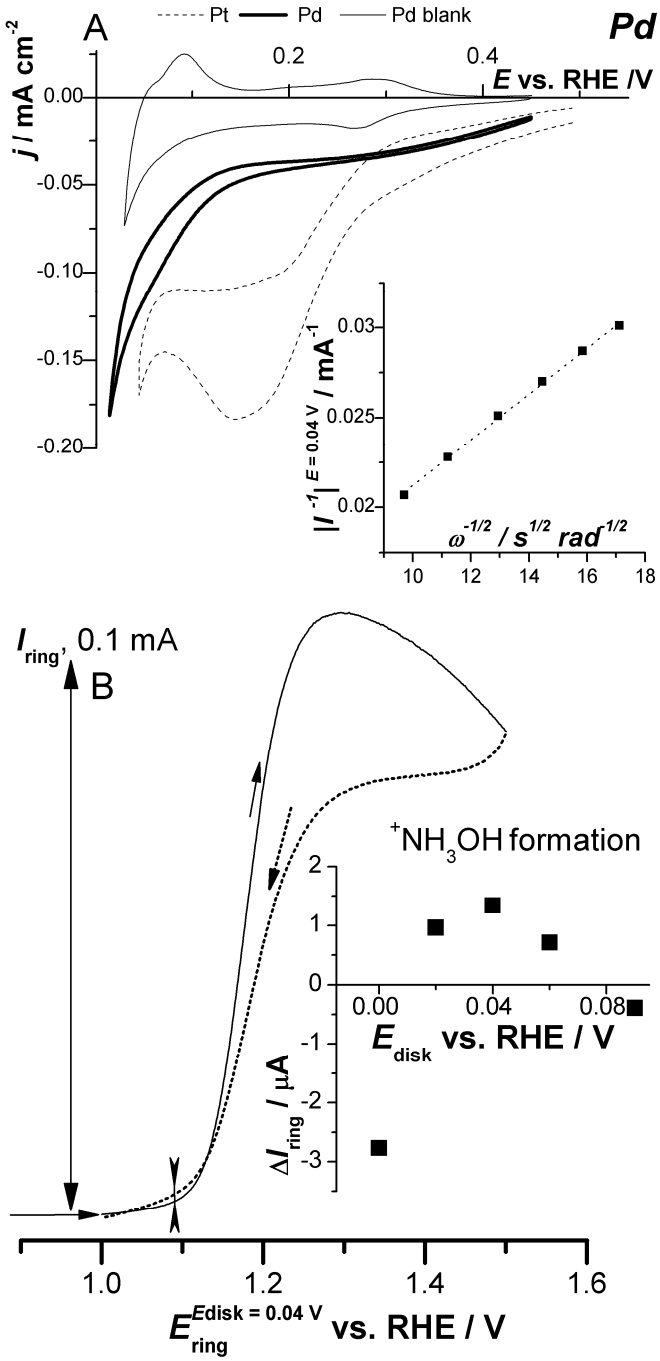
A
Pt
Pd
Pd blank
Pd
j / mA cm-2
E vs. RHE /V
0.00
-0.05
-0.10
-0.15
-0.20
0.2
0.4
|I-1|E = 0.04 V / mA-1
0.03
0.025
0.02
ω-1/2 / s1/2 rad-1/2
10
12
14
16
18
Iring, 0.1 mA
B
+NH3OH formation
2
1
0
-1
-2
-3
ΔIring / μA
0.00
0.04
0.08
Edisk vs. RHE / V
1.0
1.2
1.4
1.6
Eringdisk = 0.04 V vs. RHE / V

Figure 3 Panel A: Reduction profile of 50 μM $NaNO_2$ in 0.1 M H_2SO_4 at a rotating Pd thin layer disk electrode (bold line) compared to a rotating Pt electrode (dashed line), v = 10 mV s^{-1}, ω = 900 rpm. The thin line is the blank voltammogram of the Pd thin layer electrode for v = 20 mV s^{-1}. Inset: Koutecky-Levich plot at E_{disk} = 0.04 V. Panel B: Profile of the ring current during a shielding experiment (ω = 900 rpm, v = 10 mV s^{-1}) in 0.1 M H_2SO_4 + 0.8 mM $NaNO_2$. I_{ring} is shown as a thin line for the positive-going sweep and as dashed line for the negative-going sweep, E_{disk} = 0.04 V. The arrows indicate the direction of the potential sweep. Inset: plot of the semi-quantitative parameter ΔI_{ring} for hydroxylamine formation (see text) as a function of disk potential.

Because of the long duration of the shielding experiments (see below), a slightly less acidic supporting electrolyte was chosen to reduce the decomposition of HNO_2. The two-wave signal is clearly visible, and the effect of a changing rotation rate on the current in the region of the low-potential wave was analyzed. The disk current was fitted to the Koutecky-Levich equation (inset to figure 3A) [46] in the range 0.09 – 0.04 V,

$$\frac{1}{I_{disk}} = \frac{1}{0.62nFAc_{nitrite}D^{2/3}\nu^{-1/6}\omega^{1/2}} + \frac{1}{I_k} \qquad (1)$$

where the symbols have their usual meaning. The HNO_2 diffusion coefficient value that we use for all calculations is $1.9 \cdot 10^{-5}$ cm^2 s^{-1} [45]. The slope was found to decrease with decreasing E and n was equal to 3.6 ± 0.4 (error expressed as 2σ) when E_{disk} = 0.04 V. This value can be interpreted in terms of HNO_2 conversion to NH_3OH^+ ($n_{theoretical}$ = 4); a slightly underestimated n value was also found for Pt and Rh in similar conditions[45] (Chapters 2 and 6). Additional evidence of NH_3OH^+ formation was obtained with ring shielding experiments [46] (Chapter 2) in the disk potential range 0.00 – 0.09 V. Figure 3B shows the most important portion of the voltammogram recorded at a ring electrode during such a shielding experiment. Above 1 V, a large oxidation signal, which can be mainly ascribed to nitrite oxidation[47], dominates the voltammogram. However, if hydroxylamine generated at the disk transits to the ring, the current during the negative-going sweep (from 1.5 V backwards, dashed line in the Figure) will feature a slightly larger oxidation current than the positive-going sweep in a limited potential range (1.05 – 1 V). This is the known fingerprint of hydroxylamine in a nitrite-containing solution [45]. Figure 3B displays the response of the ring electrode when hydroxylamine is released at the disk, the potential of which is kept constant at 0.04 V. A semi-quantitative

parameter can be introduced to quantify the potential-dependent conversion of HNO_2 to NH_3OH^+, which has also been used in Chapter 8. This parameter is simply defined as:

$$\Delta I_{ring}(E_{ring}) = I_{ring}(E_{ring,negative-going}) - I_{ring}(E_{ring,positive-going}) \quad (2)$$

for a suitably chosen ring potential (in our case E_{ring} = 1.09 V). The inset to Figure 3B displays the evolution of ΔI_{ring} as a function of disk potential. A positive ΔI_{ring} indicates that NH_3OH^+ is being formed at the disk. Therefore, we can conclude that, in agreement with the shielding experiments, that selectivity to NH_3OH^+ is restricted to a narrow potential range, 0.02 – 0.06 V. Below this range, massive hydrogen evolution at the disk is the predominant reaction (accompanied by hydrogen re-oxidation at the ring); the selectivity above 0.09 V is discussed in the next section. The rather small value of ΔI_{ring} is consistent for a ca. pH 1 solution and in agreement with previous reports: hydroxylamine detection improves with higher pH [45], ΔI_{ring} increasing from 2-6 μA at pH 1.7 to 10-40 μA at pH 3 (see Chapter 8).

Finally, the electron count with Equation (1) excludes that NH_4^+ is a by-product of HNO_2 reduction at Pd at 0.04 V. However, it must be remembered that NH_4^+ cannot be oxidized at the Pt ring electrode in acidic media, and so direct observation of this molecule is not possible with RRDE [12]. Therefore, conversion of HNO_2 to NH_4^+ at a Pd electrode for $E < 0$ V cannot be completely excluded.

7.3.1.1.4 The coinage metals (Cu, Ag, Au)

Figure 4 displays the voltammetric profile of the coinage metals in acidic electrolytes and their response to the addition of $NaNO_2$. The catalytic activity follows the order Cu >> Ag ~ Au. Ag and Au both share a small but appreciable reduction current measured well before the onset of hydrogen evolution. The broad potential range where the featureless reduction signal is observed on Au (onset at E = 0.75 V) correlates well with the region where continuous NO reduction at gold electrodes has been previously reported in acidic media[35], and indicates that probably NO is at least one of the active nitrogen-containing species on gold. On the other hand, Ag could only be studied in a narrower potential range due to early oxidation of this metal, and the use of $HClO_4$ is of key importance in order to avoid adsorption of (bi)sulfate ions [48]. A reduction current appears upon addition of

$NaNO_2$, which increases with higher nitrite concentration. Similarly to gold, the reduction signal is featureless and anticipates hydrogen evolution, and the voltammetric profile in the presence of nitrite clearly deviates from the blank at around E = 0.15 V. Different to gold, when the potential is decreased even further (as far as −0.4 V, not shown in Figure), the nitrite reduction current always exceeds the hydrogen evolution current (as measured in the blank electrolyte).

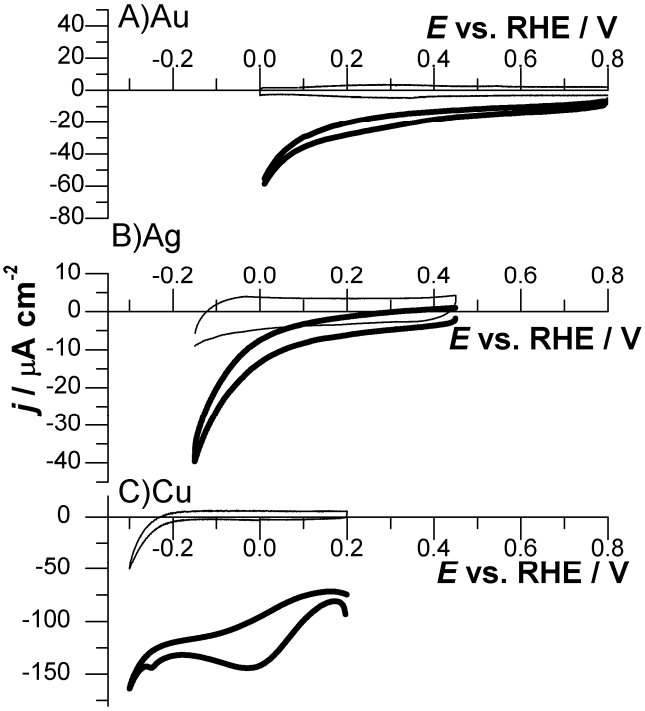

Figure 4 Voltammetric profiles for the reduction of 0.8 mM $NaNO_2$ at coinage metal electrodes, v = 20 mV s^{-1}. Panel A: Au bead, working electrolyte 0.1 M $HClO_4$. Panel B: Ag disk, working electrolyte 0.1 M $HClO_4$. Panel C: Cu disk, working electrolyte 0.1 M $HClO_4$.

Copper electrodes display a remarkably high reduction current, comparable to that of noble metals, in the entire range of the potential sweep, which was limited to E < 0.2 V to avoid copper dissolution [15]. The voltammetric profile features a broad peak with a maximum at E = 0 V and a smaller signal very close to hydrogen evolution. The broad peak shifts to more positive potentials with decreasing scan rates: this typically evidences an irreversible (multi-)electron reaction transfer[46].

7.3.1.2 On-Line Mass Spectroscopy (OLEMS).

OLEMS experiments were carried out in order to track the formation of gaseous products, such as N_2 (m/z = 28), NO (m/z = 30) and N_2O (m/z = 44), as in Chapters 2 and 6. The contribution of N_2O to the NO current has been subtracted using fragmentation tables from reference sources[49].

7.3.1.2.1 Iridium

Figure 5 shows the results of the OLEMS data for a polycrystalline Ir electrode in 0.5 M H_2SO_4 containing 0.8 mM $NaNO_2$. The voltammetric profile compares well to that of Figure 1. The MS current for NO decreases throughout the negative-going sweep and is characterized by two different slopes: a flatter region between 0.2 and 0.4 V and a steeper section at lower values. N_2O is produced mainly in the former region, with a peak around 0.3 V. This profile differs from those previously observed for Pt and Rh. For these two metals, in fact, NO is consumed in correspondence to the formation of N_2O but then the NO current reaches a constant value in the low-potential range (E < 0.15 V), where the dominant reaction is HNO_2 direct reduction (i.e. not the reduction of NO). For Ir, the presence of two slopes for m/z = 30 suggests that the same reactant, NO, is taking part in two different reaction pathways, possibly leading to two different products, suggesting that a soluble, hydrogenated product replaces N_2O as favored product in the low-potential region. Therefore, OLEMS data indicate that NO remains the main reactant for Ir also in the low-potential region.

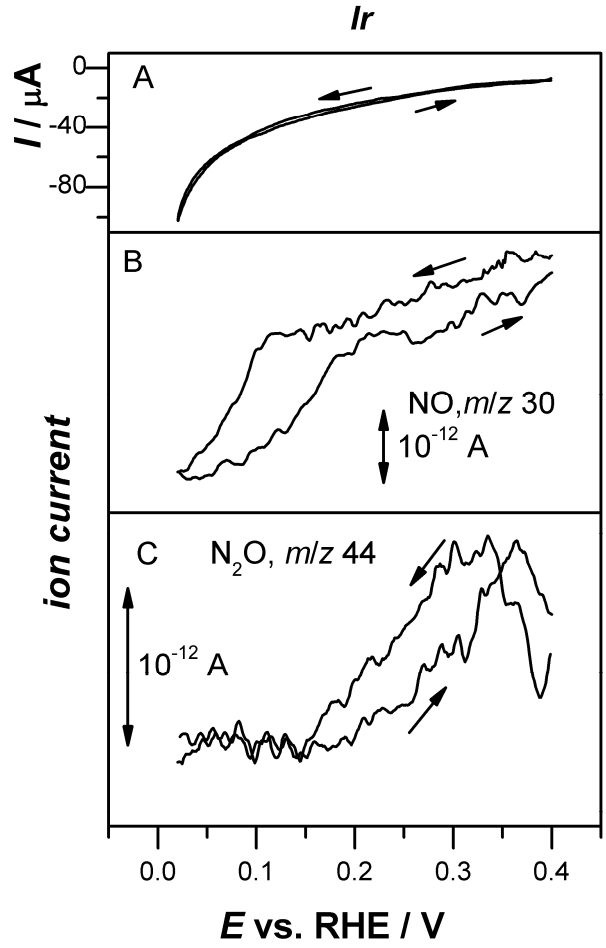

Figure 5 Cyclic voltammetry during OLEMS measurements (A) and ion current profiles for $m/z = 30$ (B) and $m/z = 44$ (C) in 0.5 M H_2SO_4 containing 0.8 mM $NaNO_2$. The working electrode is a polycrystalline Ir wire electrode, v = 1 mV s^{-1}. The arrows indicate the direction of the potential sweep.

7.3.1.2.2 Ruthenium

Ru electrodes were investigated in a somewhat larger potential window than for cyclic voltammetry (Figure 6): the likely formation of oxides was neglected because the electrode was used for a single experiment and then the Ru layer was removed. The Ru profile is characterized once more by the typical features of gas

evolution at noble metals: solution-phase NO is consumed and converted to N_2O for potentials higher than E = 0.15 V. However, differently from Ir and similarly to Pt and Rh, Ru features a low-potential region where the NO ion current is stable and that is usually associated to a shift in reactivity from solution-phase NO to direct conversion of HNO_2.

7.3.1.2.3 Thin-layer palladium on gold

Consumption of solution-phase NO with corresponding N_2O evolution was also observed for thin-layer Pd electrodes (Figure 7). The potential window of N_2O formation is broader than for other metals, extending from 0.6 V to the onset of hydrogen evolution; the decrease of the *m*/*z* 44 current is abrupt and associated with a change of the slope of the voltammetric profile; the NO mass spectrometry ion current also slowly decreases again in the lower potential range, although not as steeply as in the case of Ir (see above). We note that a two-wave voltammetric profile was associated (for Pt and Rh) to a shift to direct HNO_2 consumption at lower potentials, although in such case the NO ion current should remain constant at low potentials. The OLEMS profile for a bulk Pd electrode, limited to a lower potential of E = 0.2 V, reproduced the highly selective N_2O formation. Contrary to previous reports studying continuous NO reduction [35], N_2 evolution is below detection limits: since this gas is generated from a stepwise conversion NO → N_2O → N_2, we assume that the local partial pressure of N_2O is too limited for a sufficient amount of N_2 to be produced.

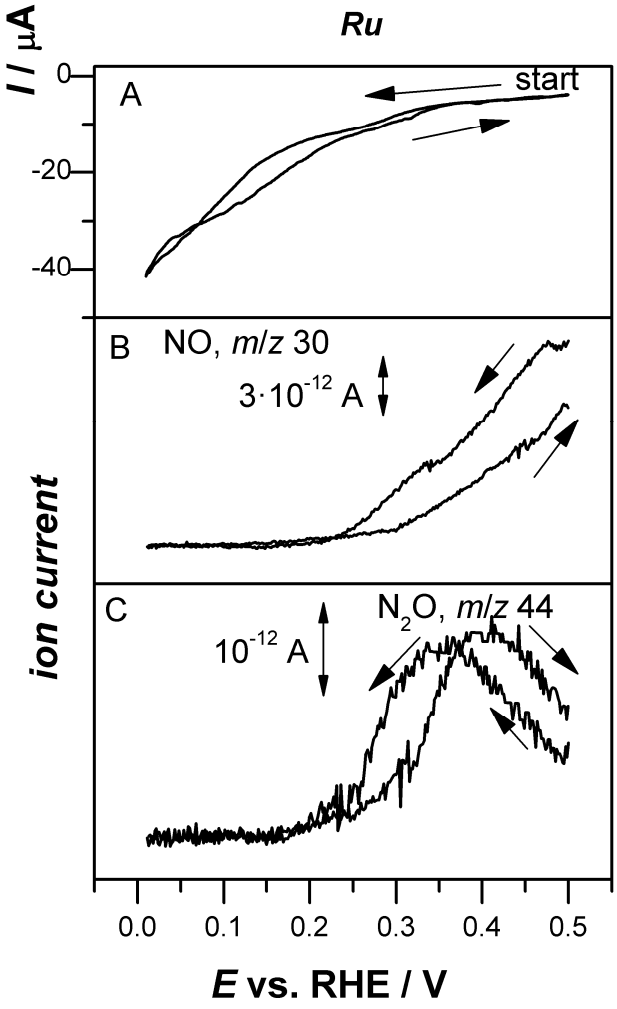

Figure 6 Cyclic voltammetry during OLEMS measurements (A) and ion current profiles for $m/z = 30$ (B) and $m/z = 44$ (C) in 0.5 M H_2SO_4 containing 0.8 mM $NaNO_2$. The working electrode is a gold bead coated with Ru, $v = 1$ mV s^{-1}. The arrows indicate the direction of the potential sweep.

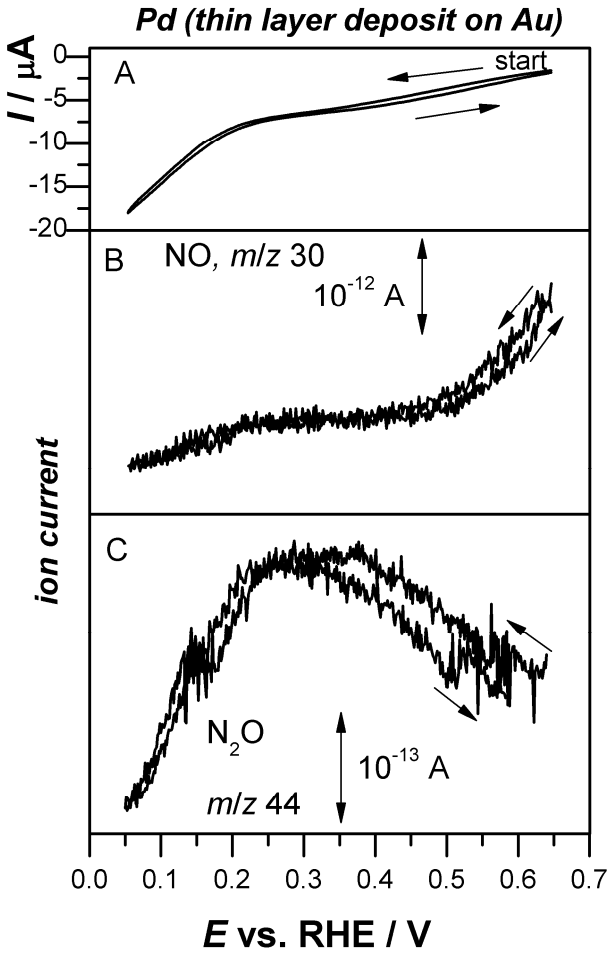

Figure 7 Cyclic voltammetry during OLEMS measurements (A) and ion current profiles for $m/z = 30$ (B) and $m/z = 44$ (C) in 0.5 M H_2SO_4 containing 0.8 mM $NaNO_2$. The working electrode is a gold bead coated with a thin Pd layer, $v = 1$ mV s^{-1}. The arrows indicate the direction of the potential sweep.

7.3.1.2.4 The coinage metals (Cu, Ag, Au)

Next, coinage metals will be discussed. Figure 8 shows that gas production on Au is characterized by a stark hysteresis between the negative-going sweep from 0.75 V and the positive-going sweep from −0.25 V. The negative-going sweep is the most straightforward to explain. NO appears as the first gaseous product around 0.5

V and thus well before any N_2O is detected: the onset potential of the evolution of nitrous oxide is 0.4 V. Both gaseous products disappear close to the onset of hydrogen evolution and thus it is reasonable to assume that the selectivity shifts to more hydrogenated, soluble products. The positive-going branch does not show the large NO peak, whereas the N_2O peak, though similar in shape to the peak recorded in the negative-going scan, is shifted to higher potential, in agreement with the shift observed in the voltammetric profile (panel A). The mass spectrometry NO ion current is characterized by a dip in correspondence with the N_2O peak, which clearly indicates that N_2O formation, that is, NO consumption, exceeds the rate of NO formation. This is not observed in the negative-going scan because NO evolution precedes the onset of N_2O formation and so a sufficient NO local partial pressure can build up at the electrode before being depleted by NO dimerization and subsequent N_2O formation [35]. The ratio between the maximum MS peak currents of N_2O and NO within the same experiment is 1/3 for Au, a number that we will compare to other NO-forming coinage metals later.

Ag features selectivity to gaseous products, similar to Au. This is clearly seen in Figure 9, where a remarkable increase in the m/z = 30 current is reported during reduction of 1.6 mM $NaNO_2$ in 0.1 $HClO_4$. Starting from the contact potential of 0.4 V, no variation of the m/z current is observed until E = 0.1 V. Similarly to Au, NO is the first gaseous product to be detected: from E = 0.1 V the NO signal departs from the baseline, peaking around −0.2 V, below which the signal begins to decrease. This reversal in the trend of the NO current may be associated to the onset of hydrogen evolution, indicated by the dashed line in the figure. N_2O is also detected in a ratio of 1/10 with respect to NO; moreover, the onset of N_2O production is located around −0.1 V. Vigorous hydrogen evolution corresponds to a rapid suppression of both NO and N_2O production, and (probably) a shift to soluble products.

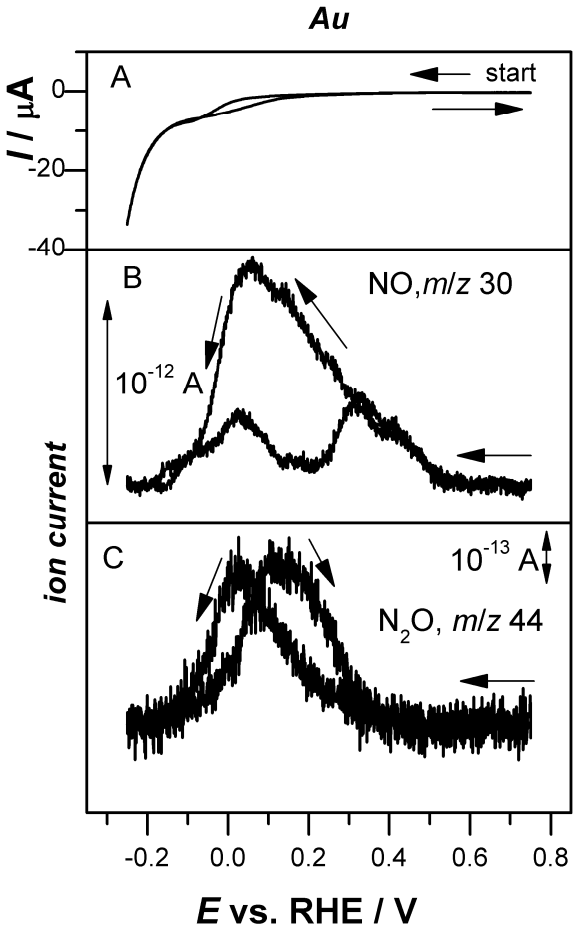

Figure 8 Cyclic voltammetry during OLEMS measurements (A) and ion current profiles for $m/z = 30$ (B) and $m/z = 44$ (C) in 0.1 M $HClO_4$ containing 1.6 mM $NaNO_2$. The working electrode is a polycrystalline Au bead electrode, $v = 1$ mV s^{-1}. The arrows indicate the direction of the potential sweep.

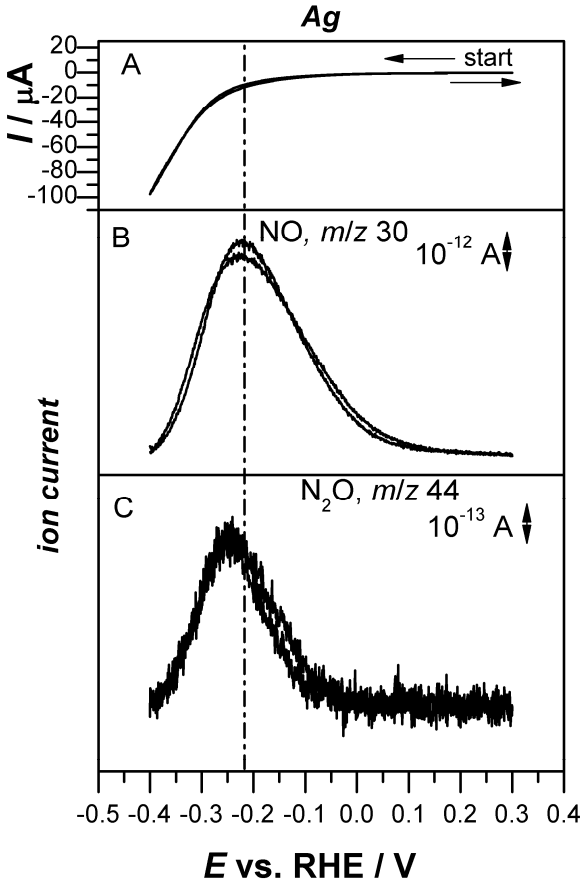

Figure 9 Cyclic voltammetry during OLEMS measurements (A) and ion current profiles for m/z = 30 (B) and m/z = 44 (C) in 0.1 M $HClO_4$ containing 1.6 mM $NaNO_2$. The working electrode is a polycrystalline Ag bead electrode, v = 1 mV s^{-1}. The dashed-dotted line indicates the onset potential for hydrogen evolution. The arrows indicate the direction of the potential sweep.

Copper electrodes were analyzed in a restricted potential range to avoid copper oxidation as much as possible, and thus the upper potential was limited to 0.275 V. As an additional precaution, the potential sweep was started in the hydrogen evolution region. Cu is peculiar in that it is the only metal to show no evolution of N_2O at all in the potential range analyzed (Figure 10). Gas formation was indeed observed for E > 0.18 V, corresponding to a sharp increase of the m/z current related to NO. It is likely that NO formation would continuously increase if the

potential were scanned up to even more positive values. Our findings are in agreement with the observed selectivity towards NO evolution at a copper electrode during NO_3^- reduction in acidic media[15]. This study ascribed NO formation to a local cell mechanism with Cu^{+2} as by-product (i.e. nitrate-induced copper corrosion), despite the fact that oxidative currents were never measured. Therefore, solution samples before and after the OLEMS experiment were analyzed with an Inductively Coupled Plasma (ICP) setup and the copper content was determined. Before the analysis, the copper concentration (c_{Cu}) is below detection limits, whereas c_{Cu} reaches 60 ppb after the experiment. We could ascribe (at least partly) NO formation to copper oxidation by nitrous acid and ensuing formation of NO and Cu^{+2} ions[15]. Additional experimental evidence would however be necessary to corroborate this hypothesis.

An increase of the electrolyte pH to 3 (0.1 M phosphate buffer) shifts the acid-base equilibrium HNO_2/NO_2^- towards nitrite, quenching the solution-phase decomposition to NO. OLEMS experiments showed that the reduced NO solution concentration caused by the higher pH leads to a decrease in the measured amount of N_2O produced at noble metal electrodes (Ir, Pd and Ru), but no change in mechanism. This effect was quantified for Rh with a semi-quantitative calibration in Chapter 6. Ag and Au, on the other hand, are characterized by a remarkable decrease in both NO and N_2O production, whereas the relative N_2O/NO ratio is conserved. This observation suggests that HNO_2 is the primary active species on Ag and Au, whereas NO_2^- has a much lower or no reactivity (see below). An increase in pH does not modify the gas evolution patterns of Cu, except for a slight negative shift of the onset potential for NO evolution (0.08 V instead of 0.18 V). This is in agreement with reports that discuss the unusually high (with respect to the other two coinage metals) electrocatalytic activity of nitrate reduction at copper electrodes in alkaline media [23,24].

An overview of gaseous products for nitrous acid reduction at polycrystalline metals is given in Table 2.

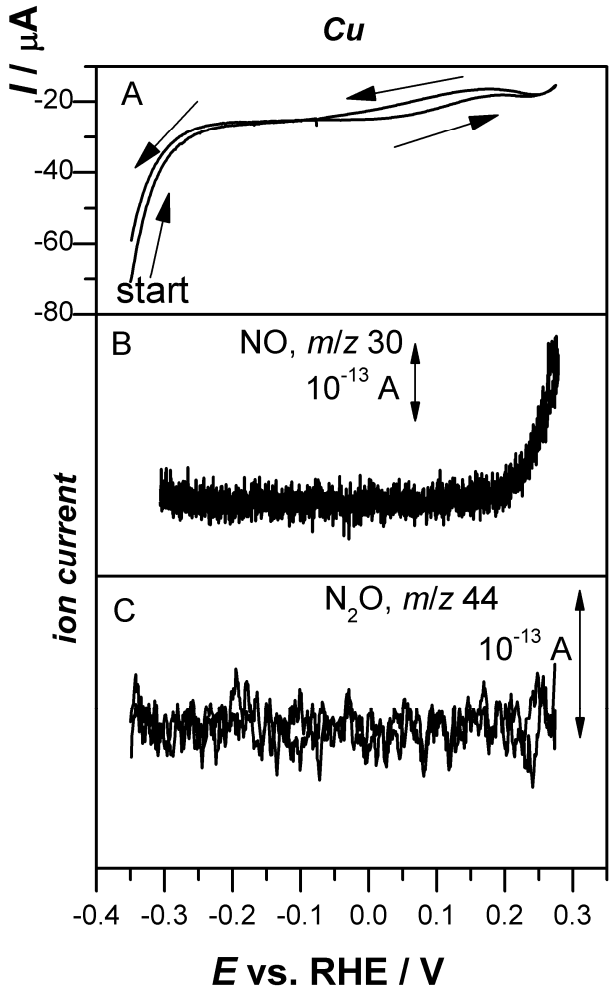

Figure 10 Cyclic voltammetry during OLEMS measurements (A) and ion current profiles for m/z = 30 (B) and m/z = 44 (C) in 0.1 M $HClO_4$ containing 1 mM $NaNO_2$. The working electrode is a polycrystalline Cu disk electrode, v = 1 mV s^{-1}. The arrows indicate the direction of the potential sweep.

7.3.2 Alkaline media

7.3.2.1 Iridium

The voltammetry of a polycrystalline Ir electrode in a nitrite-containing 0.1 M NaOH solution is shown in Figure 11. The choice of the upper potential limit at 0.4

V is explained above (Section 6.3.1.1) to ensure that no Ir oxides are formed. The voltammetric features shown in the blank voltammogram are reproducibly obtained with the flame-annealing technique. Two couples of reversible peaks can be seen, located at 0.12 and 0.23 V, along with a broad, minor feature above 0.3 V. Although the two couples of reversible peaks are likely to be ascribable to hydrogen UPD, the assignment of these peaks to a precise surface process or surface site is not possible due to the absence of related information in the literature. Most experiments with Ir, in fact, do not involve bulk polycrystalline electrodes but Ir deposits on a support[39] or non-flame annealed wires[50], and their focus is mainly on the anodic behavior of Ir or its oxides. The addition of nitrite to the solution leads to the appearance of reduction signals, characterized by a smaller reduction current density than for acidic media for the same nitrite concentration. The voltammetric profile is dominated by a broad reduction peak located at 0.21 V, while at lower potentials the features of hydrogen adsorption are discernible and possibly overlapped with some other reduction process. Therefore, cyclic voltammetry does not allow us to claim that Ir is completely poisoned by H_{upd}, at least not to the same extent as for Pt under identical conditions (Chapter 2), where the poisoning is much more clear-cut. An increase of nitrite concentration as displayed in Figure 11 demonstrates that the current increases by a very minor amount upon a tenfold increase of nitrite concentration, indicating that the kinetic order is low. A Tafel slope analysis was carried out by employing a stepped potential program (steps of 10 mV min^{-1}) in a special cell where the counter electrode was located in a separate compartment, equipped with a glass frit, to ensure that any possible product released at the counter electrode did not interfere with the measurements at the working electrode. The Tafel slope region extends from 0.38 V to 0.24 V and covers approximately 1 current decade; within this region, the Tafel slope value equals (130 ± 4 mV), a slope sufficiently close to the theoretical value of 120 mV to conclude that the first electron transfer is rate determining. This result agrees with the Tafel slope for Rh stationary electrodes under identical conditions (Chapter 6). The Tafel slope obtained during the positive-going scan coincides with the value of negative-going staircase within the observed error bars, and no poisoning is observed.

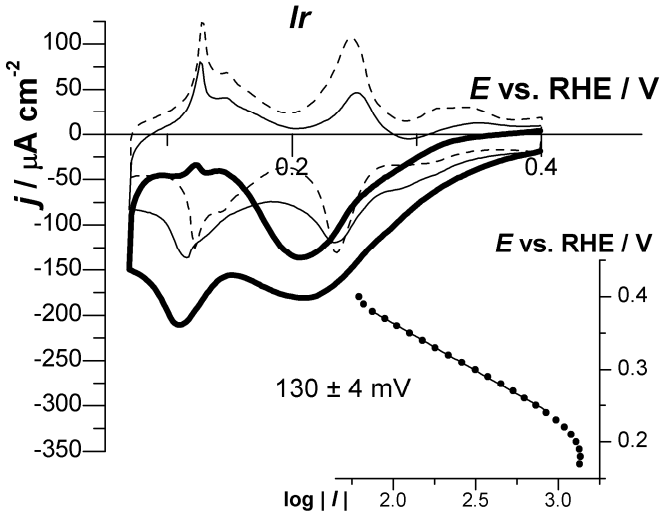

Figure 11 Voltammetric profiles for the reduction of increasing $NaNO_2$ concentrations in 0.1 M NaOH at a polycrystalline Ir electrode, compared to blank voltammogram (dashed line). Thin line: 90 μM, thick line 0.9 mM, v = 20 mV s^{-1}. Inset: polarization curve and Tafel slope for nitrite reduction, potential program 10 mV min^{-1}.

7.3.2.2 Ruthenium

Ruthenium electrodes are characterized by a peak-shaped signal with no low-potential poisoning due to H_{upd} (Figure 12): this voltammetric profile closely resembles that of a polycrystalline rhodium electrode (Chapter 6). As expected for irreversible processes, the peak potential shifts to more positive values with lower scan-rates [46]. Evidence concerning the rate-determining step can also be obtained by recording a Tafel slope as described above for iridium electrodes, which yields a value of 110 ± 1 mV. This value indicates that, as for Ir and Rh, the first electron transfer is the rate-determining step, that is the reaction

$$NO_2^- + e^- + H_2O \rightarrow NO_{ads} + 2OH^- \qquad (3)$$

A further analysis of the voltammetric features can supply additional mechanistic information. A linear relationship between the peak current I_p and $v^{1/2}$ is valid throughout the scan rate range investigated and indicates once more that nitrite reduction on ruthenium electrodes is an irreversible multi-electron partially

diffusion-limited process. The number of electrons exchanged in the process, n, may be calculated from the following equation[46]

$$I_p = -(2.99 \cdot 10^5) n(\alpha n^*)^{1/2} A D_{NO2-}^{1/2} v^{1/2} c_{NO2-} \quad \text{(A)} \tag{4}$$

To our knowledge, the value of D for the nitrite ion in 0.1 M NaOH is not available in the literature, in contrast to HNO_2, whose diffusion coefficient is $1.9 \cdot 10^{-5}$ cm^2 s^{-1} [45]. Uncertainties in D_{NO2-} will inevitably cause uncertainty affecting n in Equation (4). Piela et al. have pointed out that the value of the diffusion coefficient of NO_2^- is likely smaller than D_{HNO2} [47]. However, values decreasing from $3.67 \cdot 10^{-5}$ for a pH 4 phosphate buffer [51] to $1.33 \cdot 10^{-5}$ cm^2 s^{-1} for a neutral solution (0.1 M Na_2SO_4)[47] have been reported. If we use the latter estimation of D_{NO2-}, equation (4) yields $n = 3.2 \pm 0.1$. Therefore, we can conclude that nitrite reduction on a Ru deposit, as suggested by the comparison to other noble metals, definitely proceeds beyond NO to give a more reduced product, whose identification is not possible by the electron count via equation (4) alone.

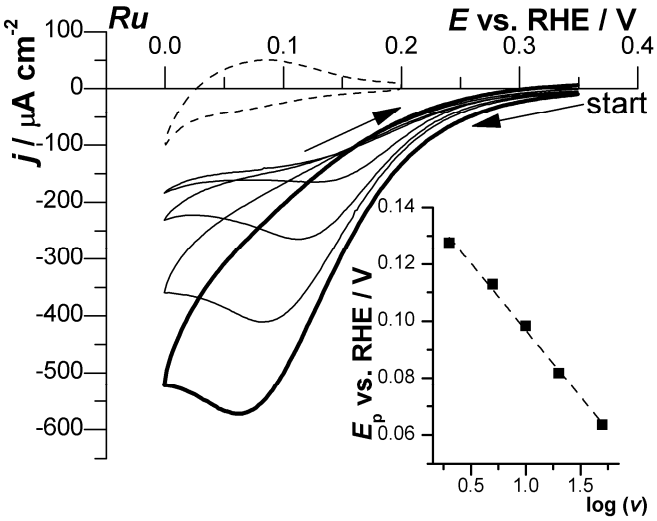

Figure 12 Voltammetric profiles for the reduction of 0.8 mM $NaNO_2$ in 0.1 M NaOH at a thin-layer Ru electrode for various scan rates (50-20-10-5 mV s^{-1}). v = 50 mV s^{-1} for the thick line. The arrows indicate the direction of the potential sweep. Inset: linear relationship between E_p vs. log (v).

7.3.2.3 Coinage metals (Cu, Ag, Au)

Gold and silver show no appreciable reactivity towards the reduction of nitrite in alkaline media at potentials preceding hydrogen evolution, in agreement with previous reports[11,20]. Nitrite reduction on copper electrodes in alkaline media has been thoroughly discussed in the literature [23,24]. Reyter et al. have shown that Cu, which is by far the most active of the three coinage metals, is characterized by a stepwise conversion to of nitrite to ammonia, hydroxylamine being identified as the intermediate. Poisoning by H_{ads} occurs close to hydrogen evolution[23].

7.3.2.4 OLEMS experiments

OLEMS experiments of Ru and Ir were also carried out. No gaseous product was ever detected, in agreement with our findings discussed in Chapters 2 and 6. However, a well-ordered Pt (100) electrode represent a remarkable exception, because it converts nitrite to N_2 directly in a narrow but well-defined potential range in 0.1 M NaOH (Chapters 3,4,5).

7.4. Discussion

This section will first deal with the discussion of the product selectivity of the metals studied in acidic and alkaline media and will highlight peculiar properties of each metal. A general discussion of nitrite/nitrous acid reduction at polycrystalline metals will be given afterwards.

7.4.1 Acidic media

Table 1 shows the details of direct HNO_2 reduction at each metal, obtained throughout the thesis.

Metal	**Direct HNO_2 reduction ?**	**Notes**
Ru	Yes	$HNO_2 \rightarrow NO_{ads} \rightarrow (NH_4^+)$. $E < 0.1$ V
Rh	Yes	$HNO_2 \rightarrow NH_4^+$ (diffusion-controlled) $0.05 < E < 0.1$ V

Ir	No	NO is the favored reactant in acidic media as shown by OLEMS data. Direct HNO_2 reduction cannot be excluded on the basis of our experimental evidence. Either NH_4^+ or NH_3OH^+ is the product. $E < 0.1$ V
Pd	Yes	$HNO_2 \rightarrow NH_3OH^+$ (mixed control) $0.02 < E < 0.06$ V
Pt	Yes	$HNO_2 \rightarrow NH_3OH^+$ (diffusion-controlled)[45]. $0.05 < E < 0.1$ V
Cu	Yes	Open-circuit copper corrosion by HNO_2 may contribute to NO evolution.[15]
Ag	Yes	$HNO_2 \rightarrow$ NO (the thermodynamically stable product of NO_3^- reduction[52])
Au	Yes	$HNO_2 \rightarrow$ NO

Table 1 Overview of the electrocatalytic activity of polycrystalline metals towards direct HNO_2 reduction in acidic media.

7.4.1.1 N_2O evolution and NO adlayer.

Table 2 summarizes the details of gas evolution at the different metal electrodes.

Metal	**N_2O evolution in acidic media ?**	**Notes, and *E* range of N_2O formation**
Ru	Yes	$0.2 < E < (0.5)$ V
Rh	Yes	$0.2 < E < (0.6)$ V
Ir	Yes	$0.15 < E < (0.4)$ V
Pd	Yes	Very broad N_2O signal, extending

		close to the H_{UPD} region. $0.10 < E < (0.6)$ V
Pt	Yes	$0.2 < E < (0.6)$ V
Cu	*No*	NO only gas product.
Ag	Yes	NO is the major gas product. N_2O/NO ratio is 1/10. $-0.35 < E < -0.1$ V.
Au	Yes	NO is the major gas product. N_2O/NO ratio is 1/3 $-0.15 < E < 0.4$ V (negative-going sweep)

Table 2 Overview of the evolution of gaseous products at polycrystalline metal electrodes during electrocatalytic reduction of an acidic nitrite solution. Potentials given in brackets are equivalent to the upper limit potential of voltammetric scans in the present study and may not correspond to the actual upper limit of N_2O evolution.

The mechanism of N_2O formation[35], reported in its overall form as Equation (5) below, involves the presence of NO adsorbed at the surface and NO in the solution:

$$NO_{ads} + NO_{aq} + 2H^+ + 2e^- \rightarrow N_2O + H_2O \quad (5)$$

This reaction is not characterized by a strong influence of the nature of the metal, as already proposed in studies addressing the reduction of solution-phase NO [11,14]: N_2O evolution occurs in a comparable potential region for a wide range of metal displaying otherwise different characteristics: Pd, Au, Ru, Ir. A few peculiarities of the separate metals will now be discussed.

7.4.1.1.1 Iridium

First of all, Ir shows two important characteristics: a preference for reacting with NO in acidic media and a large degree of poisoning due to NO adsorption (Section 7.3.1.1.1). NO is adsorbed molecularly and with a high coverage on Ir (110) [27] but on Ir (100) and (111) [26] a certain degree of dissociation was detected by in-situ

FTIR. In addition, Weaver et al. have studied an Ir thin film deposited on a roughened Au surface with SERS [28]: their work showed that Ir displays the typical vibration of atop NO_{ads}, along with a weaker signal that was ascribed to bridge-bonded NO_{ads}. The band ascribed to the NO adsorbate was found to decrease with more negative potential, but the presence of a band at 570 cm^{-1}, assigned to Ir-O vibrations, suggested that NO partly dissociates at the surface, this process being enhanced at low potentials. In fact, this "poisoning" species could not be removed at -0.2 V vs. RHE[28]. Accordingly, the poisoning we noticed after NO adsorption from an acidic nitrite solution may be ascribed to NO dissociation. As for product assignment, spectroelectrochemical experiments at single-crystal Ir electrodes highlighted that NO_{ads} could be converted to NH_x species, whose typical band at 1450 cm^{-1} was detected[26,27] . Therefore, it seems reasonable to assume that in the low-potential region, NH_4^+ or NH_3OH^+ is formed from NO reduction. Direct HNO_2 reduction cannot be completely excluded on the basis of our experimental evidence.

7.4.1.1.2 Ruthenium

Ruthenium is another highly oxophilic metal[41,43]. Yan et al. [29] have highlighted the fact that NO coadsorbs with oxygen species (Ru oxides) when a Ru electrode is immersed in an NO-saturated solution. The "stripping" of the NO adlayer coincides with the reduction of the surface oxides for potentials below 0.3 V. In the presence of nitrite in the acidic electrolyte, however, re-adsorption of NO onto metal sites was observed below E = 0.3 V [29]. Our OLEMS measurements indicate that there is indeed a low-potential region (E < 0.2 V, Figure 6) where the Ru electrode stops consuming solution-phase NO. The simultaneous absence of NH_3OH^+ formation indicates that NH_4^+, the only other soluble product, must be formed at Ru electrodes in this low potential region. Given the strong Ru-NO interaction, we suggest that a stepwise mechanism $HNO_2 \rightarrow NO_{ads} \rightarrow NH_4^+$ is operative.

7.4.1.1.3 Thin layer palladium on gold

The unusually large window of N_2O formation on Pd has already been observed during continuous NO reduction by De Vooys et al. [35]. A lower onset potential of NO_{ads} stripping on Pd with respect to Pt has been found in this work (Section 7.3.1.1.3) and in the literature [35]. These observations indicate that the broader potential window where selectivity to N_2O predominates can be ascribed to an

intrinsically stronger Pd – NO bond, which is however not accompanied by NO dissociation [53]. Consequently, when a sufficiently low potential is reached, N_2O evolution eventually stops and the selectivity shifts to NH_3OH^+ in a very narrow potential range, before H_2 evolution starts interfering.

7.4.1.2 NO evolution on coinage metals

The selectivity between the two nitrogen oxides shifts from N_2O to NO in the order Au < Ag << Cu, where the latter metal reduces HNO_2 only to NO. Since mechanism (5) also applies to coinage metals in saturated NO solutions[35], the simplest explanation of the behavior of coinage metals lies in their weaker metal-NO interaction [53]. Contrary to noble metals, when Ag or Au is immersed in the NO-containing acidic nitrite solution no well-defined NO adlayer forms and the very small amount of solution-phase NO of an acidic nitrite solution is not sufficient for reaction (5) to be observed (a saturated NO solution is approximately 3 mM). Consequently, only when a sufficiently high local partial pressure of NO is formed, N_2O evolution starts. In fact, if NO is externally supplied as reactant (and saturates the electrolyte) Au typically behaves as a transition metal, converting NO to N_2O in a broad potential range [35]. In our case, we suggest that a stepwise mechanism is operative, with reaction (6)

$$HNO_2 + H^+ + e^- \rightarrow NO_{aq/ads} + H_2O \qquad (6)$$

preceding NO recombination (reaction (5)). NO can escape from the electrode surface (thanks to a weak affinity toward coinage metals) and be detected. As for N_2O formation, recent research for Cu (under UHV conditions [54]) and Ag has highlighted that an NO dimer is the intermediate: theoretical calculations [55] and gas-phase experiments [52] have shown that NO is a stable intermediate product of HNO_3 reduction at silver under vacuum conditions and further conversion to N_2O requires the formation of $(NO)_2$ in the presence of a (Lewis) acid catalyst (Ag^+ and/or H^+). This may be the reason why the removal of H^+ by vigorous hydrogen evolution will further suppress the pathway leading to N_2O and the selectivity will eventually shift to soluble products. It must be noted that, generally speaking, N_2 and NH_4^+ are the expected thermodynamically stable products of NO_3^- reduction in acidic solutions [11].

7.4.2 Alkaline media

Table 3 presents a summary of the peculiarities of each metal toward the reduction of nitrite anions in alkaline media.

Metal	Reactivity towards NO_2^-	Notes
Ru	Yes	$NO_2^- + e^- + H_2O \rightarrow NO + 2OH^-$ is r.d.s. Hydrogenated product formed.
Rh	Yes	$NO_2^- + e^- + H_2O \rightarrow NO + 2OH^-$ is r.d.s. Formation of NH_3 via intermediate NH_2OH. Poisoning due to N_{ads} formation from NH_3 reoxidation
Ir	Yes	$NO_2^- + e^- + H_2O \rightarrow NO + 2OH^-$ is r.d.s. Evidence of poisoning owing to competition with H_{UPD}
Pd	Yes	Surface-confined reaction speculated[56] $H_{ads} + NO_2^-{}_{ads} \rightarrow$ products
Pt	Yes	NH_2OH formed on polycrystalline Pt, evidence of poisoning ascribed to competition with H_{UPD} (100) domains : direct conversion to N_2
Cu	Yes	Diffusion-controlled reaction to NH_3. Various intermediate surface species postulated. [23,24]
Ag	*No*	Very high overpotential. Reduction of nitrite occurs simultaneously with hydrogen evolution. [20]
Au	*No*	NO is reported to be the only active nitrogen species on Au in alkaline media.[57]

Table 3 Overview of the electrocatalytic activity of polycrystalline metals towards direct NO_2^- reduction in 0.1 M NaOH.

Transition metals exhibit the following order in activity towards nitrite reduction in alkaline media: Rh ~ Ru > Pt > Ir. Tafel slope analysis indicates that on Ir, Ru and Rh (see Chapter 6) the rate-determining step is the first electron transfer that converts NO_2^- into NO. The latter molecule is adsorbed on the metal surface and is quickly converted to hydrogenated products. The absence of N_2O evolution further suggests that NO is strongly adsorbed (or converted too rapidly) and is never released into the solution. A detailed identification of the final product of nitrite reduction was not carried out, but we can speculate that Ru, featuring a peak current density comparable to that of Rh in the same conditions, will completely reduce NO_2^- to NH_3.

7.4.3 General discussion of reactivity trends of polycrystalline metals

Due to the presence of solution-phase NO during reduction of HNO_2, the reactivity trends of polycrystalline metals in acidic media will be heavily influenced by thermodynamic parameters of NO adsorption. The NO-surface bond was discussed by Brown and King [53] in terms of molecular orbitals involved in the NO-metal interaction and a close similarity to the CO-metal system was identified. In brief, DFT calculations[58] suggested that the CO-metal bonding is dominated by $2\pi^*$-d and 5σ-d mixed-bonding states with a strong d character. As d-band energy levels increase when we move from IB to VIA metals, the $2\pi^*$-d overlap is progressively enhanced with an increased population of bonding $2\pi^*$-d states, thus strengthening the NO-metal interaction but weakening the internal N-O bond and consequently enhancing the tendency of NO to dissociate. Transition metals in the left side of the Periodic Table (in our case Ir, Ru) will strongly bind NO and, on the one hand, convert it to N_2O (as all other noble metals) and on the other (partly) dissociate the adsorbate. This process, which usually leads to a poisoning of the metal surface, is particularly visible for Ir, as discussed above. Metals pertaining to groups in the center of the transition metal region of the Periodic Table are less prone to dissociate NO, though still able to bind NO and convert it to N_2O (Rh, Pt and Pd); additionally, the complete removal of NO from Rh, Pt and Pd allows the metal surface to be "clean" at low potentials and can directly reduce HNO_2 (see Table 1). Our results also indicate that there is a clear-cut relation between the ability to dissociate NO and the conversion of NO_2^- to NH_3, which rests on the cleavage of

all N-O bonds (see Chapter 6). The inability of a metal to dissociate NO will be mirrored by the appearance of NH_2OH among the products (one N-O bond conserved), while the formation of NH_3 seems to require ability to dissociate NO as prerequisite. Pd and Pt do not feature NO dissociation[53] and in turn are the only two metals producing NH_2OH as a product of nitrite reduction. Finally, coinage metals feature a low NO adsorption energy (80 kJ mol^{-1} have been reported for NO on Cu , 45-65 kJ mol^{-1} for NO on Ag (111) [53], compared to an average of 200 kJ mol^{-1} for noble metals). The reactivity towards HNO_2 will be limited and NO produced can be released from the surface (Tables 1 and 2).

According to the well-known Sabatier principle[59], we would expect an exceedingly strong or weak NO binding to penalize the reactivity of a certain metal. Indeed, only intermediate cases such as Pt, Pd and Rh show a clear two-stage reaction: first, the N_2O formation region, then, close to incipient hydrogen evolution, a direct conversion of HNO_2 to NH_3OH^+ and NH_4^+ (see Tables 1 and 2). This 4- or 6-electron reaction is possible only on NO-free surfaces: adsorbed NO inhibits the reaction [60] or interferes with it, as in the case of Ru.

The scarcity of available thermodynamic data concerning nitrite interaction with metal surfaces does not allow us to support the observed trends in alkaline media with quantitative data from theory or experiment. However, general observations can still be made by starting from these two criteria:

- Appreciable nitrite reduction activity (Table 3)
- Occurrence of H_{UPD} poisoning. (Table 3).

We can thus list the parameters that can potentially be used to rationalize the reactivity trends in alkaline media:

- *NO adsorption energy* (NO is an intermediate of nitrite reduction in alkaline media and it is a product of the rate-determining step (3)).
- *NO_2^- adsorption energy* (unavailable in the literature)
- *Potential of zero (free) charge*, which could indicate which metals feature a stronger interaction to anions. This parameter has however been determined for very few metals in alkaline media. If we compare the

reactivity trends to available pz(f)c data, Rh, reported to have a lower potential of zero (free) charge than Pt[61], is also the more active of the two metals and does not show any poisoning due to H_{UPD} (Chapter 6).

- *Work function*, which is a more widely available quantity and is closely related to potentials of zero free charge. If the simple linear relationships proposed by Trasatti are used [62], Rh and Ru, having a similar work function, will have a lower potential of zero free charge than Pt, which is consistent with the higher electrocatalytic activity toward nitrite reduction. However, Ir is rather inert even though its work function is comparable to that of Ru and Rh.

7.5. Conclusions

The reduction of nitrite at various noble and coinage metals has been studied in acidic and alkaline media. In acidic media, the main focus was on gaseous products: all noble metals react with solution-phase NO (from HNO_2 decomposition) to give N_2O in a common potential window. The affinity of the metal to NO chemisorption determines the metal's behavior at lower potentials following the Sabatier principle: a high affinity to NO leads to poisoning, partly via NO fragmentation (Ir, Ru), while an intermediate NO adsorption energy represents the optimum (Pt, Rh); the NO adlayer on these metals can easily be removed and direct, diffusion-controlled reaction of HNO_2 takes place at lower potentials. Coinage metals, characterized by a weak NO adsorption energy, have a limited catalytic activity and follow a different pathway: $HNO_2 \rightarrow NO \rightarrow N_2O$, the latter gas being generated only when a sufficient local partial pressure of NO has been reached. Reactivity trends in alkaline media follow the order Rh ~ Ru > Pt > Ir with a common rate-determining step: the first electron transfer $NO_2^- + e^- + H_2O \rightarrow NO_{ads} + 2OH^-$. The least reactive noble metals suffer from a competition with H_{UPD} at lower potential, while a stronger affinity to NO helps the metal to overcome this competition.

7.6. Acknowledgements

We acknowledge partial financial support from the European Commission (through FP7 Initial Training Network "ELCAT", Grant Agreement No. 214936-2). M.T.M.K. acknowledges financial support from the Netherlands Organization for

Scientific Research ("NWO-Middelgroot") for the purchase and development of the online electrochemical mass spectrometer.

References.

(1) Canfield, D. E.; Glazer, A. N.; Falkowski, P. G. *Science* **2010**, *330*, 192-196.
(2) Galloway, J. N.; Townsend, A. R.; Erisman, J. W.; Bekunda, M.; Cai, Z. C.; Freney, J. R.; Martinelli, L. A.; Seitzinger, S. P.; Sutton, M. A. *Science* **2008**, *320*, 889-892.
(3) Manassaram, D. M.; Backer, L. C.; Moll, D. M. *Environ. Health Perspect.* **2006**, *114*, 320-327.
(4) Moorcroft, M. J.; Davis, J.; Compton, R. G. *Talanta* **2001**, *54*, 785-803.
(5) Hiscock, K. M.; Lloyd, J. W.; Lerner, D. N. *Water Res.* **1991**, *25*, 1099-1111.
(6) Almasri, M. N. *Environ. Impact Assess. Rev.* **2007**, *27*, 220-242.
(7) Mateju, V.; Cizinska, S.; Krejci, J.; Janoch, T. *Enzyme Microb. Technol.* **1992**, *14*, 170-183.
(8) Soares, M. I. M. *Water, Air, Soil Pollut.* **2000**, *123*, 183-193.
(9) Kapoor, A.; Viraraghavan, T. *J. Environ. Eng.-ASCE* **1997**, *123*, 371-380.
(10) Fanning, J. C. *Coord. Chem. Rev.* **2000**, *199*, 159-179.
(11) Rosca, V.; Duca, M.; de Groot, M. T.; Koper, M. T. M. *Chem. Rev.* **2009**, *109*, 2209-2244.
(12) de Vooys, A. C. A.; van Santen, R. A.; van Veen, J. A. R. *J. Mol. Catal. A: Chem.* **2000**, *154*, 203-215.
(13) Yang, J.; Duca, M.; Schouten, K. J. P.; Koper, M. T. M. *J. Electroanal. Chem.* **2011**, *662*, 87-92.
(14) de Vooys, A. C. A.; Beltramo, G. L.; van Riet, B.; van Veen, J. A. R.; Koper, M. T. M. *Electrochim. Acta* **2004**, *49*, 1307-1314.
(15) Dima, G. E.; de Vooys, A. C. A.; Koper, M. T. M. *J. Electroanal. Chem.* **2003**, *554-555*, 15-23.
(16) da Silva, G.; Kennedy, E. M.; Dlugogorski, B. Z. *J. Phys. Chem. A* **2006**, *110*, 11371-11376.
(17) *Handbook of Chemistry and Physics*; 53rd ed. ed.; Weast, R. C., Ed.; The Chemical Rubber, co.: Cleveland, 1972-1973.
(18) Park, J. Y.; Lee, Y. N. *J. Phys. Chem.* **1988**, *92*, 6294-6302.
(19) Pletcher, D.; Poorabedi, Z. *Electrochim. Acta* **1979**, *24*, 1253-1256.
(20) Cattarin, S. *J. Appl. Electrochem.* **1992**, *22*, 1077-1081.
(21) Davis, J.; Moorcroft, M. J.; Wilkins, S. J.; Compton, R. G.; Cardosi, M. F. *Analyst* **2000**, *125*, 737-741.
(22) Bouzek, K.; Paidar, M.; Sadilkova, A.; Bergmann, H. *J. Appl. Electrochem.* **2001**, *31*, 1185-1193.
(23) Reyter, D.; Belanger, D.; Roue, L. *Electrochim. Acta* **2008**, *53*, 5977-5984.
(24) Badea, G. E. *Electrochim. Acta* **2009**, *54*, 996-1001.
(25) Aouina, N.; Cachet, H.; Debiemme-chouvy, C.; Thi, T. M. T. *Electrochim. Acta* **2010**, *55*, 7341-7345.
(26) Gomez, R.; Weaver, M. J. *J. Phys. Chem. B* **1998**, *102*, 3754-3764.
(27) Gomez, R.; Weaver, M. J. *Langmuir* **1998**, *14*, 2525-2534.

(28) Zou, S. Z.; Gomez, R.; Weaver, M. J. *Langmuir* **1997**, *13*, 6713-6721.
(29) Yan, Y. G.; Huang, B. B.; Wang, J. Y.; Wang, H. F.; Cai, W. B. *J. Catal.* **2007**, *249*, 311-317.
(30) Nakata, K.; Doi, Y.; Kubota, S.; Shimazu, K. *J. Electroanal. Chem.* **2010**, *647*, 187-193.
(31) Lai, S. C. S.; Koper, M. T. M. *Faraday Discuss.* **2008**, *140*, 399-416.
(32) Leung, L. W. H.; Weaver, M. J. *Langmuir* **1988**, *4*, 1076-1083.
(33) Tang, J.; Petri, M.; Kibler, L. A.; Kolb, D. M. *Electrochim. Acta* **2005**, *51*, 125-132.
(34) de Vooys, A. C. A.; Koper, M. T. M.; van Santen, R. A.; van Veen, J. A. R. *Electrochim. Acta* **2001**, *46*, 923-930.
(35) de Vooys, A. C. A.; Koper, M. T. M.; van Santen, R. A.; van Veen, J. A. R. *J. Catal.* **2001**, *202*, 387-394.
(36) Wonders, A. H.; Housmans, T. H. M.; Rosca, V.; Koper, M. T. M. *J. Appl. Electrochem.* **2006**, *36*, 1215-1221.
(37) Ahmadi, A.; Evans, R. W.; Attard, G. *J. Electroanal. Chem.* **1993**, *350*, 279-295.
(38) Losiewicz, B.; Martin, M.; Lebouin, C.; Lasia, A. *J. Electroanal. Chem.* **2010**, *649*, 198-205.
(39) Juodkazyte, J.; Sebeka, B.; Stalnionis, G.; Juodkazis, K. *Electroanalysis* **2005**, *17*, 1734-1739.
(40) Motoo, S.; Furuya, N. *J. Electroanal. Chem.* **1984**, *167*, 309-315.
(41) Rand, D. A. J.; Michell, D.; Woods, R. *J. Electrochem. Soc.* **1977**, *124*, C131-C131.
(42) Colucci, J. A.; Foral, M. J.; Langer, S. H. *Electrochim. Acta* **1985**, *30*, 1675-1685.
(43) Juodkazyte, J.; Vilkauskaite, R.; Sebeka, B.; Juodkazis, K. *Trans. Inst. Met. Finish.* **2007**, *85*, 194-201.
(44) Koper, M. T. M. *Electrochim. Acta, In Press, Corrected Proof.*
(45) Gadde, R. R.; Bruckenstein, S. *J. Electroanal. Chem.* **1974**, *50*, 163-174.
(46) Bard, A. J.; Faulkner, L. R. *Electrochemical methods : fundamentals and applications*; 2nd ed. ed.; John Wiley & Sons: New York, 2001.
(47) Piela, B.; Wrona, P. K. *J. Electrochem. Soc.* **2002**, *149*, E55-E63.
(48) Horanyi, G.; Rizmayer, E. M.; Konya, J. *J. Electroanal. Chem.* **1984**, *176*, 339-348.
(49) *NIST Chemistry WebBook, NIST Standard Reference Database Number 69*; Linstrom, P. J.; Mallard, W. G., Eds. Gaithersburg MD, 20899, http://webbook.nist.gov, retrieved February 18, 2010.
(50) Jaksic, M. M.; Johansen, B.; Tunold, R. *Int. J. Hydrogen Energy* **1994**, *19*, 321-335.
(51) Kamyabi, M. A.; Aghajanloo, F. *J. Electroanal. Chem.* **2008**, *614*, 157-165.
(52) Zangmeister, C. D.; Davis, R. J.; Mrozek, P.; Pemberton, J. E. *Surf. Sci.* **2008**, *602*, 2395-2401.
(53) Brown, W. A.; King, D. A. *J. Phys. Chem. B* **2000**, *104*, 2578-2595.
(54) Haq, S.; Raval, R. *Phys. Chem. Chem. Phys.* **2007**, *9*, 3641-3647.
(55) Liu, Z. P.; Jenkins, S. J.; King, D. A. *J. Am. Chem. Soc.* **2004**, *126*, 7336-7340.
(56) Denuault, G.; Milhano, C.; Pletcher, D. *Phys. Chem. Chem. Phys.* **2005**, *7*, 3545-3551.
(57) Suzuki, S.; Nakato, T.; Hattori, H.; Kita, H. *J. Electroanal. Chem.* **1995**, *396*, 143-150.
(58) Koper, M. T. M.; van Santen, R. A.; Wasileski, S. A.; Weaver, M. J. *J. Chem. Phys.* **2000**, *113*, 4392-4407.

(59) *Catalysis: An Integrated Approach*; 2nd ed. ed.; van Santen, R. A.; Moulijn, J. A.; Averill, B. A.; van Leeuwen, P. W. N. M., Eds.; Elsevier Science b.v. : Amsterdam, 2000.
(60) Rodes, A.; Gomez, R.; Orts, J. M.; Feliu, J. M.; Perez, J. M.; Aldaz, A. *Langmuir* **1995**, *11*, 3549-3553.
(61) Frumkin, A. N.; Petrii, O. A. *Electrochim. Acta* **1975**, *20*, 347-359.
(62) Trasatti, S. *J. Electroanal. Chem.* **1971**, *33*, 351-378.